

Development of a ceramic membrane for emulsion water-diesel treatment

N. Kamoun^{1*}, F. Jamoussi¹, M. A. Rodríguez²

¹Water Researches and Technologies Center, Georesources Laboratory, Borj Cedria Ecopark, BP 273, 8020 Solima, Tunisia

²Instituto de Cerámica y Vidrio, Madrid, Spain

Abstract

The purpose of this study was the development of a low-cost ceramic tubular membrane, using inexpensive materials, namely natural clay, and graphite as a porogenic agent. Such a low-cost membrane can be used as filters or porous supports for the preparation of multilayer ceramic membranes. Extrusion was used as a shape-forming method for this purpose. Graphite was selected as a porogenic additive. Raw materials were physicochemically and morphologically characterized. A comparative study of the influence of porogen content on membrane characteristics was carried out. Finally a graphite addition of 15 wt% and 850 °C as the sintering temperature were chosen. The obtained membrane had 41 vol% of porosity, diametral compression strength of 4 MPa, and relatively good corrosion resistance in basic and acid conditions. The performance of the membrane support was evaluated for diesel-in-water emulsion depuration as a function of pressure. Filtration test using 15% of porogen sample led to turbidity rejection factor of 95%. Therefore, it was considered that this membrane can be suitable for diesel/water emulsion treatment.

Keywords: clay, graphite, membrane, oil emulsion.

INTRODUCTION


In the field of maritime transport, large volumes of water contaminated with diesel and other oils are generated, which must not be discharged into the sea. Several technologies have been developed for the treatment of water/diesel emulsions, adsorbents, and additives to break emulsions. Membrane technology has received increasing attention over the last 10 years, with potential applications in many fields. Membrane separation is currently considered one of the most promising technologies due to low power consumption, the possibility of continuous operation, chemical and mechanical stability, drastically lower investment cost, ease of operation, and ultimately, its cost-effectiveness. Initially, membrane separation technology was confined to a laboratory scale. However, the improvements of the last twenty years have expanded its application at an industrial level. The use of membranes for the removal of emulsions is a simple method and membranes have been commonly recognized as ideal materials for treating various types of emulsions [1].

The development of new ceramic formulations, together with simple manufacturing techniques, could play an important role in the preparation of low-cost membranes. Generally, most ceramic membranes are prepared from alumina (Al₂O₃) [2], zirconia (ZrO₂) [3-5], and alumina with titanium oxide (TiO₂) [6]. However, the application of ceramic membranes is highly restricted by the high cost of both starting materials and sintering, due to the required high temperatures. In addition, it should be noted that the average

price of alumina and zirconia-based ceramic membranes is in the range of 500 to 3,000 \$/m² [7]. Nevertheless, there is a huge opportunity to prepare ceramic membranes with low-cost raw materials while retaining their advantages. Vinoth et al. [8] estimated the manufacturing cost of 0.339 μm pore-sized kaolin-based membrane as 69 \$/m². For this reason, many research works are now focusing on the raw materials for membrane manufacturing that are chosen based on their high local abundance as clays [9-10], bentonite clay, dolomite, and others. Ceramic membranes prepared from these raw materials have excellent thermal, chemical, and mechanical stability comparable to commercially available ceramic membranes at a much lower cost, gaining immense popularity. The production of a high porosity level requires porogenic agents that have shown potential results. During heating, the organic particles are burned up to the firing temperature, leaving voids in the ceramic body. The morphology of these voids relies upon the selected porogenic agent and can be controlled by the particle size distribution. A large number of porogenic agents have been studied, including sucrose [11], starch [12-13], lycopodium [14], and so forth.

In Tunisia, clays are used in a wide range of applications by the ceramic industry [15-19]. One of the points for the development of the Tunisian economy is considered to be the exploitation and valorization of local raw materials. This study focuses on the development of novel membrane support by the addition of graphite to the raw material (clay from Tunisia). Extrusion was used as a shape-forming method and the sintering step was adjusted to the lowest possible temperature. The developed membrane supports were characterized by their porosity, pore size distribution, mechanical strength, permeate flux, and rejection performance. They have also

*kamounnaoufel@yahoo.fr

 <https://orcid.org/0000-0003-1515-9148>

been tested for their performance in the diesel-water emulsion treatment.

EXPERIMENTAL PROCEDURE

Characterization of raw materials: the clay used as raw material was collected from a quarry of Sidi El Bader, region of Tabarka (northwest Tunisia), and graphite powder (99.6%, Sofacel, Spain) was used as a porogenic agent due to its two special characteristics: total removal by combustion during sintering, and generation of gases during the first stage of sintering, preventing the closure of the pores. The graphite had an average particle size d_{50} of 1.71 μm and a specific surface area S_s of 27 m^2/g . Clay characterization is described elsewhere [20]. In order to determine its mineralogical composition, X-ray diffraction (XRD) was carried out (Xpert High, PanAnalytical) with $\text{CuK}\alpha$ radiation, at 50 kV voltage and 30 mA current. The scan was in a 2θ interval between 2° and 70° with steps of 0.05° and a counting time of 3 s/step. Thermal analysis TGA-DTA (thermogravimetry-differential thermal analysis) was performed (Setsys Evolution, Setaram, France) under an air atmosphere from room temperature (RT) to 1100 $^\circ\text{C}$ using a heating rate of 10 $^\circ\text{C}\cdot\text{min}^{-1}$. The textural study and the specific surface area measurements were carried out by N_2 adsorption (Autosorb1, Quantachrome, USA). The granulometric analysis of raw materials was made by laser scattering in aqueous dispersion (Mastersizer S, Malvern, England). The Casagrande method was selected for the determination of Atterberg limits. The experimental error was $\pm 3\%$ in accordance with Spanish standard UNE103-103-94.

Preparation and characterization of membranes: to obtain the ceramic paste, the raw materials were prepared, first grinding the clay and sieving below 65 μm then adding the graphite at different ratios (G_0 0 wt%, G_1 5 wt%, G_2 10 wt%, G_3 15 wt%, and G_4 20 wt%, Table I), and finally, the appropriate amount of water was added to obtain the desired plasticity. The mixing was carried out using a paddle stirrer to obtain a homogeneous distribution of water throughout the paste. Before the extrusion phase, an aging stage of the aqueous ceramic paste is essential to obtain a good homogeneity and promote the formation of porosities. This step is necessary to prepare a composition with rheological properties allowing shaping by extrusion. For this purpose, the resulting paste was kept in a closed plastic bag for 24 h to avoid premature drying and to ensure a homogeneous distribution of water and organic additives. After aging, the pastes were extruded and dried at room temperature for 24 h. The membrane was prepared by extrusion to obtain tubular-shaped products. A designed and homemade piston extruder (ICV-CSIC) was used. The latter consisted of a pneumatic piston, made up of a cylinder (Pneumax, Italy) with a 50 mm diameter and 200 mm piston stroke. Obtained pieces were dried in air at room temperature on rotating aluminum rolls for 24 h. This slow drying step was carried out to avoid the appearance of cracks, which can appear due to the different

capillary suction produced by the different pore sizes of the support. Membranes were then sintered in a high-temperature furnace (Agni, Germany). The heating program included an increase in temperature at 2 $^\circ\text{C}/\text{min}$ up to 250 $^\circ\text{C}$ (slow heating was carried out to avoid cracks in the support), followed by a plateau of 2 h for the complete elimination of volatile components, and a second heating step at 5 $^\circ\text{C}/\text{min}$ up to the sintering temperature, with a dwell for 2 h. Then porous components of tubular configuration (outer diameter of 8 mm and inner diameter of 4 mm) were obtained.

Table I - Different compositions for ceramic support preparation.

Mixture	Clay content (wt%)	Graphite content (wt%)
G_0	100	0
G_1	95	5
G_2	90	10
G_3	85	15
G_4	80	20

Measurements of water absorption (open porosity) were carried out according to the ASTM standard. Each value represented the average of measurements made on five individual specimens. Water absorption was estimated by the difference in the weight between the dried samples and water-saturated ones (immersion in boiled water for 3 h). Water absorption (WA, %) values were assessed by:

$$\text{WA} = \frac{m_i - m_s}{m_s} \cdot 100 \quad (\text{A})$$

where m_i (g) is the mass after the adsorption test and m_s (g) is the dry mass of the sample [21]. The porosity of the optimal composition and thermal treatment was characterized using mercury porosimetry (Autopore II 9215, Micromeritics, USA). The mechanical strength was determined using a diametral compression test. For this purpose samples had a length of about 15 mm. Each value represented the average of measurements made on ten individual specimens. For these tests, a universal testing machine with a 5000 N cell was used (Instron, UK). The diametral compression (σ , MPa) values were assessed by:

$$\sigma = \frac{P \cdot K_4}{(D_e - D_i) \cdot t} \quad (\text{B})$$

where P is the fracture load, D_i is the internal diameter, D_e is the external diameter, t is the support height, and K_4 is a constant that depends on the D_i/D_e ratio [22]. Tangential filtration tests were carried out using a pilot laboratory scale filter (Fig. 1) at 25 $^\circ\text{C}$ with flow control through an electric pump. The water flux through the support was measured versus different transmembrane pressure values.

Characterization of effluent: the composition of the effluent treated was a diesel/water emulsion: for 1 L of solution, 1 g of diesel with 0.01 g of surfactant (sodium

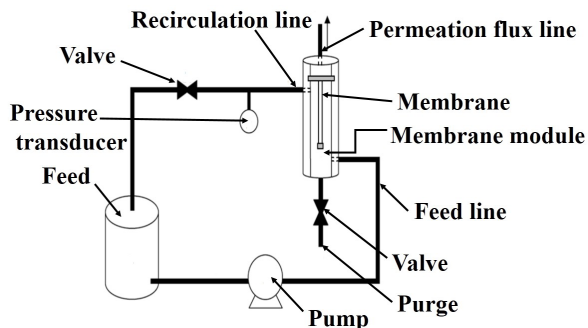


Figure 1: Schematic representation of cross-flow microfiltration setup.

dodecylbenzene sulfonate, SDBS), to improve the formation of an emulsion between two immiscible liquids. To generate the emulsion, the solution was treated with a mixer for 15 min at a rotational speed between 2500 and 3000 rpm. Turbidity was the physicochemical parameter that was determined to evaluate the efficiency of purification through the membrane, using a turbidimeter (TN-100/T-100, Oakton Instr., USA).

RESULTS AND DISCUSSION

Characterization of clay and graphite powders: Fig. 2 shows the XRD patterns of clay at room temperature and heated at temperatures tested as possible sintering temperatures (800, 850, and 900 °C). At 25 °C diffraction

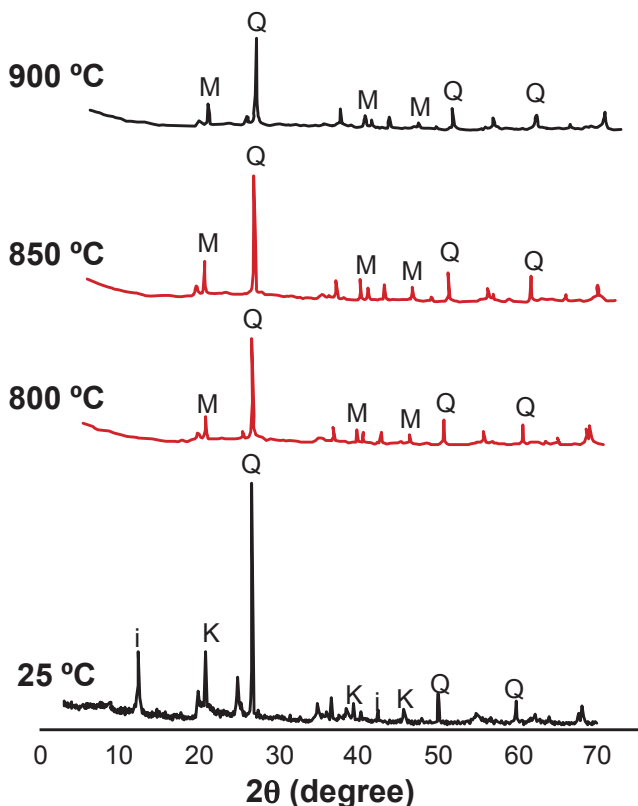


Figure 2: X-ray diffraction patterns for the raw clay sintered at various temperatures.

pattern showed essentially kaolinite and illite, with the presence of some impurities, mainly quartz. During heating, kaolinite and illite peaks disappeared by removing hydroxyl groups from the silicate network. The peaks of metakaolin and quartz were visible after the thermal treatments.

Fig. 3 shows the position of raw clay on the Holtz and Kovacs diagram, related to the plasticity parameters. It can be observed that the raw clay can be considered plastic clay according to the literature (plasticity index $IP > 15\%$). The low plastic limit (liquid limit $LL = 51\%$) has an important technological application, as it indicates the minimum percentage of water required in a clay body to reach the plastic state for its extrusion forming process [23]. From the diagram of Holtz and Kovacs, the crude clays belong to the illitic-kaolinitic domain with high plasticity. This result was consistent with XRD composition results.

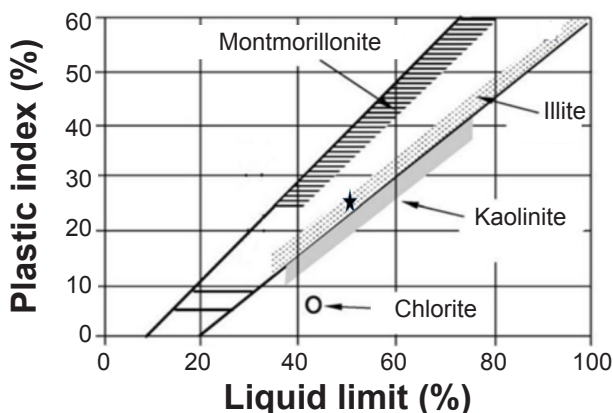


Figure 3: Position of the studied clay (indicated with a star) on the Holtz and Kovacs diagram.

From the TGA-DTA study of clay (Fig. 4a), the most interesting thermal transformations distinguished were: i) the first was located at 120 °C, which was an endothermic peak corresponding to the evaporation of the adsorbed water; ii) the second was located at 550 °C that corresponded to the dehydroxylation of the clay mineral, which implied the destruction of the kaolinite structure; iii) the third was an exothermic peak at about 960 °C that can be attributed to the phase transformation and the beginning of mullite formation. The disappearance of metakaolin was according to the mineralogical and chemical composition of the original mixture. In the graphite TGA-DTA test, graphite oxidation starting at 540 °C was detected (Fig. 4b). Also, the presence of an exothermic peak at about 716 °C corresponding to the maximum combustion rate was observed.

Fig. 5 shows particle size distribution curves of raw materials. The clay had a uniform particle size distribution with a maximum at around $d_{50} = 3.9 \mu\text{m}$. The particle size distribution of graphite showed a mono-modal distribution, with $d_{50} = 1.7 \mu\text{m}$. The specific surface area of clay obtained was much higher ($27 \text{ m}^2/\text{g}$) than the theoretical specific surface area that we can measure for this granulometry; this was due to the strong agglomeration of clay. This significant

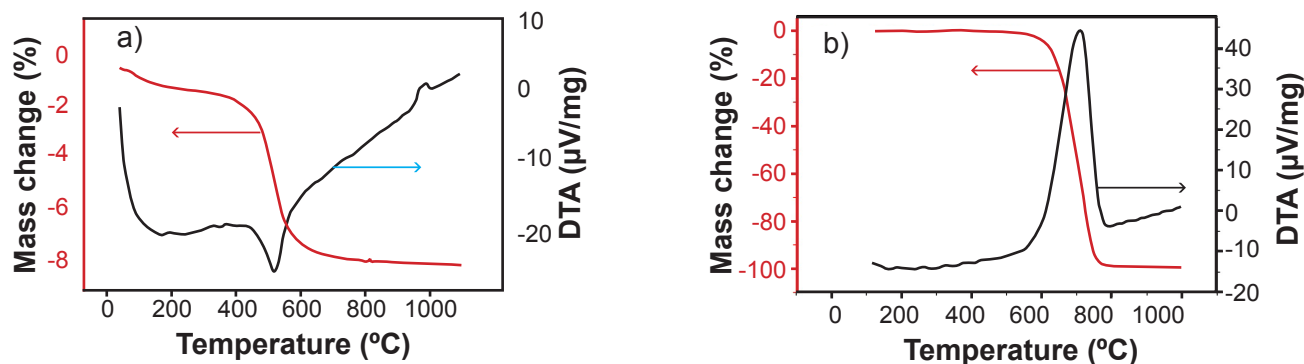


Figure 4: TGA-DTA plots of raw materials: a) clay; and b) graphite.

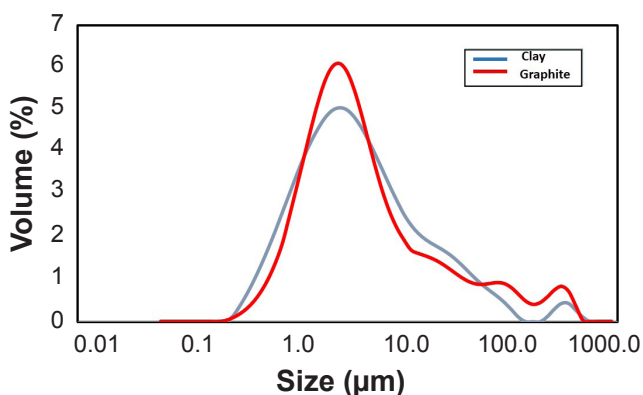


Figure 5: Particle-size distribution curves of raw materials.

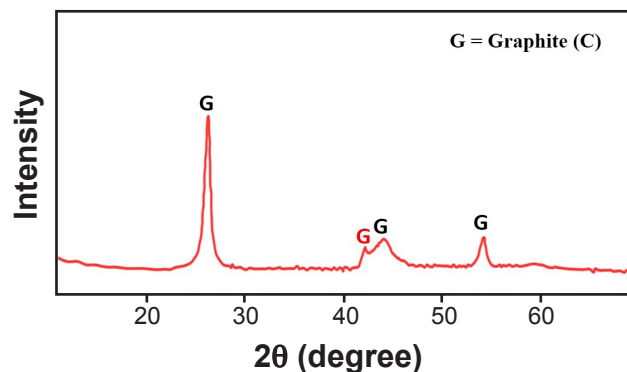


Figure 6: XRD pattern of graphite.

specific area did not make a problem. During the extrusion process, the sliding of the sheets took place, which allowed the destruction of the agglomerates.

The X-ray diffraction pattern of graphite is shown in Fig. 6. It allowed us to verify the graphite as the only component of this material. Three characteristic graphite diffraction peaks revealed the existence of pure graphite with reflection (101) at 3.35 Å.

Characterization of ceramic membrane: the supports were sintered at 800, 850, and 900 °C in air. The temperature selection was based on the previous results obtained by high-temperature microscopy and dilatometry. Within this range, porous supports may be obtained, thus avoiding the glassy phase [24]. The pore-forming agent is, therefore, totally degraded at this temperature, while the membrane consolidation through liquid phase sintering is ensured.

A relatively slow heating rate (5 °C/min) was needed in order to avoid the formation of cracks in the support due to the escape of gases from the combustion of graphite and water due to the dehydroxylation process. The evolution of porosity as a function of sintering temperature (Table II) showed that G₂ sintered at 900 °C and G₃ sintered at 850 °C had the highest porosity (41%). Similar results were reported in the literature for the increase in porosity with an increase in the amount of the porogen [25-26].

Table II - Summary of results of porosity (vol%) from ceramic support prepared with different graphite contents and sintering temperatures.

Mixture (% graphite)	800 °C	850 °C	900 °C
G ₀ (0 wt%)	32±2	36±2	27±2
G ₁ (5 wt%)	28±2	27±2	25±2
G ₂ (10 wt%)	27±2	37±2	41±2
G ₃ (15 wt%)	27±2	41±2	29±2
G ₄ (20 wt%)	28±2	30±2	30±2

In addition, the results concerning the porosity values in G₀, as a function of the sintering temperature, showed that for the sintering temperature of 800 and 850 °C the porosity revealed a negligible increase, which could be attributed to the expansion of gases of dehydroxylation. At 900 °C, the value of the porosity of G₀ decreased, associated with the densification. All the compositions with graphite had lower porosities at 800 °C (27-28 vol%), probably due to the fact that the combustion of the graphite freed up a path for the exit of gases from the dehydroxylation of the clay and therefore allowed greater shrinkage. In composition G₂, the porosity continued to increase with temperature. The porosity can be closed by the appearance of glassy phases. In the G₃ composition, the same thing happened, but above 850 °C this greater porosity allowed faster gas evacuation and predominance of sintering. In sample G₄, after the removal of such a high amount of graphite, the exit of the gases was easier and only maintenance of the porosity volume with temperature was observed. On the other hand, the mechanical strength had an opposite behavior as it decreased with the graphite percentage. These expected results confirmed the view that the loss of the organic matter

at temperatures above 570 °C was at the origin of part of the porosity.

The evolution of the mechanical strength related to the sintering temperature is shown in Fig. 7. The strength increased as temperature increased; this result was in agreement with the trend observed in the literature [24]. This was associated with the processes of neck formation between the particles, the first stage of the sintering process. Samples containing graphite as the porogenic agent had lower mechanical strength values at all the temperatures (Fig. 7) due to their high porosities. The mechanical strength decreased with the percentage of graphite up to 2.0 MPa with 20% of graphite at 900 °C. Higher porosity following the increase in graphite percentage made the membrane less resistant mechanically. Taking into account porosity and mechanical resistance, the 15% graphite support sintered at 850 °C was selected to perform filtration experiments, considering the behavior of mechanical resistance and porosity. Such resistance is estimated sufficient for emulsion filtration testing.

Chemical stability was quantified in terms of net mass loss evaluation, after membrane drying by immersion in acid and alkali solutions, individually, for a controlled time period (Fig. 8). The tubular supports were tested for their corrosion resistance using solutions of NaOH (pH 13) and

HCl (pH 1.5). In general, the mass loss increased with the time of the attack. It should be noted however that, regardless of the time of the attack in basic environments, mass loss was negligible. After 24 h, the mass loss amounted to 0.25%, while in acid a decreased mass of about 0.7% after 24 h and 1.75% after 50 h was observed. Hence, the developed materials exhibited an acceptable and sufficient mechanical strength [27].

The scanning electron microscopy (SEM) images of ceramic support G₃ at an 850 °C sintering temperature are shown in Fig. 9. The results indicated a single distribution model of the pore size and a homogeneous particle dispersion was visible. Fig. 10 illustrates the pore size distribution of

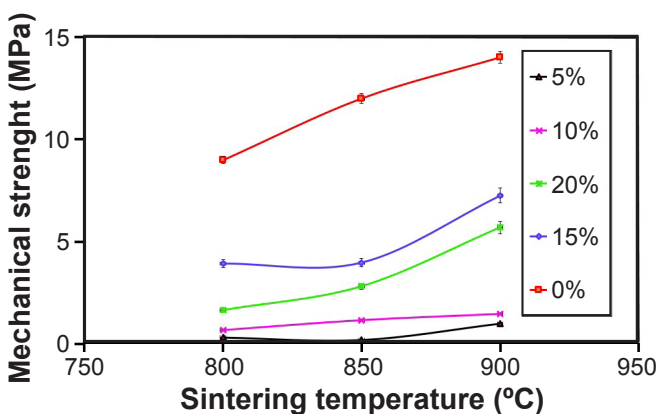


Figure 7: Mechanical strength ($\pm 5\%$) evolution versus temperature of treatment for mixtures with different graphite contents.

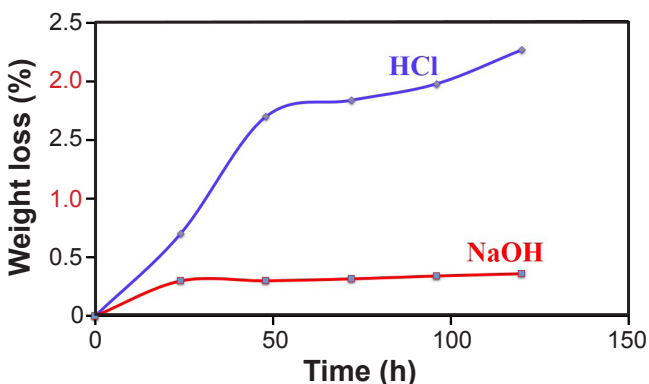


Figure 8: Chemical resistance plotted as weight loss versus time for the ceramic support in different media.

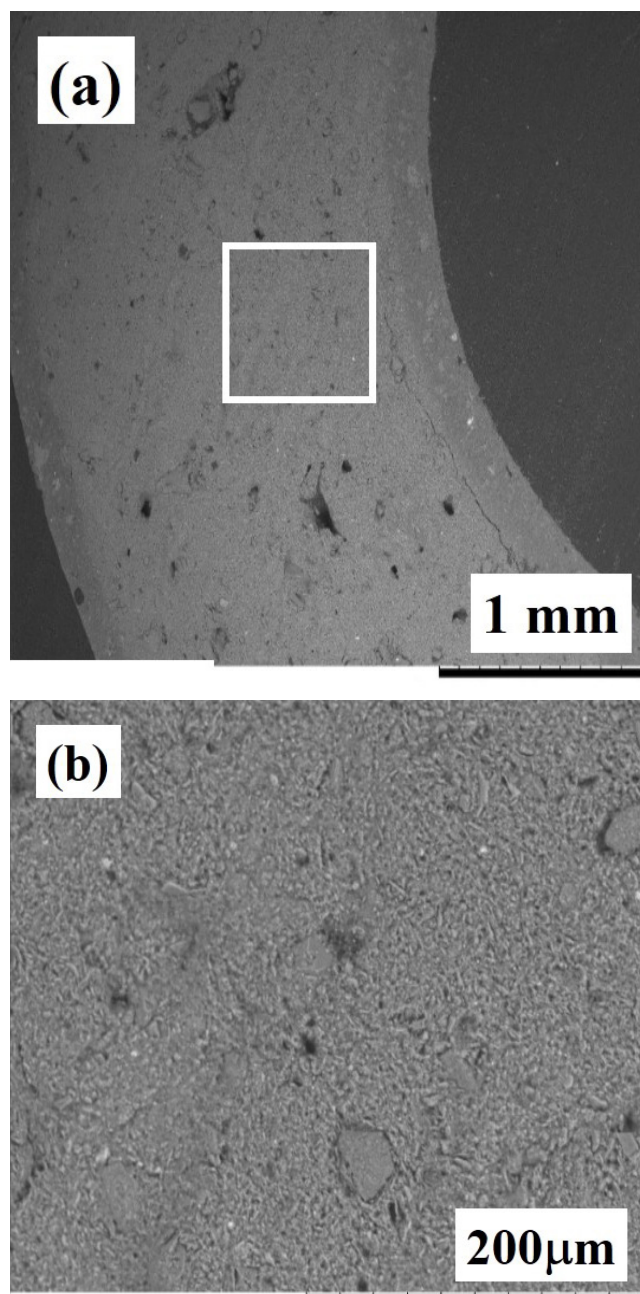


Figure 9: SEM images of ceramic support tube G₃: a) cross-section view; and b) surface view

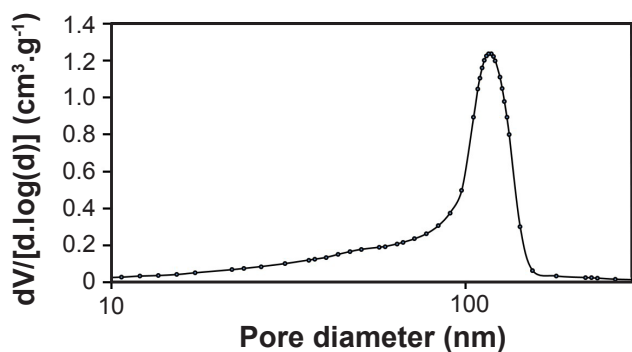


Figure 10: Pore size distribution curve of ceramic support tube G3 sintered at 850 °C.

ceramic support. Porous tubular support G₃ sintered at 850 °C had a pore size of more than 100 nm (average).

Permeation study of distilled water: the membrane water flux was evaluated using tap water (Fig. 11). The water fluxes were measured at an applied pressure of 1 bar for 1 h. It should be noticed that the flux decreased rapidly in the first 20 min, with a stable flux being obtained after 30 min. By comparing the results attained for these support membranes with those obtained previously with support made only of clay [20], it was found that the permeability was much higher compared to support without a porogenic agent. The permeability was found to be quite low even at high pressure (15 bar), while the flux values obtained were higher in membranes prepared with similar natural clays mixed with 10% cellulose as a porogenic agent. This can be explained by the porosity structure created by the cellulose fibers in the membrane support [28].

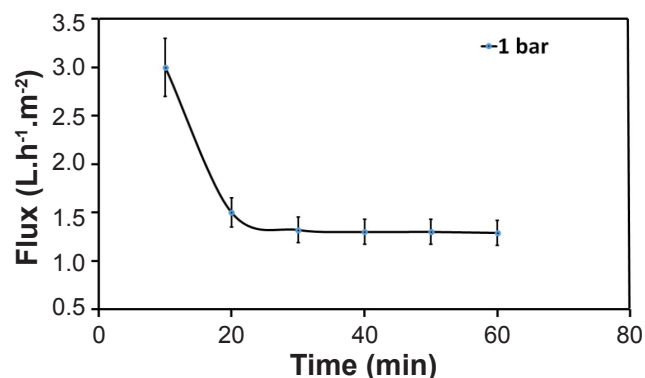


Figure 11: Flux of distilled water through the support with 15% of graphite sintered at 850 °C versus time at a 1 bar pressure.

Permeation study of emulsion water/diesel by a ceramic membrane: diesel/water emulsion filtration was carried out to evaluate the tubular support efficiency as a semi-permeable barrier. After each experiment, membranes were cleaned with sodium hydroxide (NaOH), and the system was rinsed with distilled water before and after each washing. Fig. 12 shows the flow variation of the diesel/water emulsion according to the 0 to 3 bar transmembrane pressure range. The permeate flux increased linearly with transmembrane pressure up to a value of 2.5 bar and then

stabilized at a value of 35 L.h⁻¹.m⁻². The permeate flux decreased by only 14%. This behavior can be explained by the formation of a concentrated polarization layer. The effect of the use of graphite can be markedly comparing the results obtained for this ceramic support with those obtained previously with support made only from clay [20]. In the present case, the permeability was considerably higher than the permeability of samples without graphite; this was due to the lower volume of porosity and the smaller pore size. Performance was identified in terms of permeate flow and efficiency to reduce the content of pollutants evaluated in terms of turbidity [29]. The characteristics of the emulsion diesel/water effluent before and after filtration are reported in Table III. The results were very interesting; it was possible to observe a very significant reduction in turbidity (around 95%) responsible for the discoloration of the effluent.

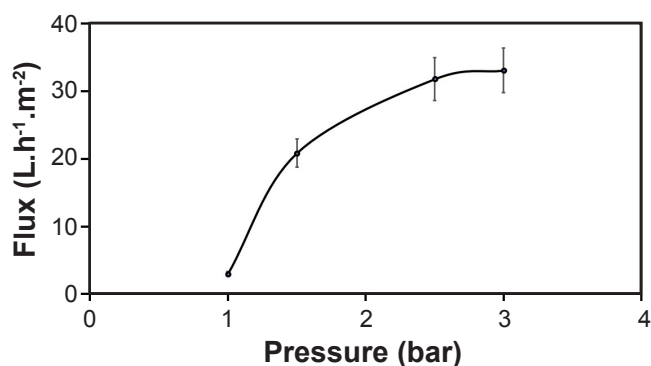


Figure 12: Flux of emulsion diesel/water through the support with 15% of graphite sintered at 850 °C versus transmembrane pressure.

Table III - Characterization of effluents before and after treatment.

Effluent	Turbidity (NTU)	Coloration
Before filtration	436	Yellowish
After filtration	2.4	Without color

CONCLUSIONS

The clay-based tubular membrane was prepared with a uniform pore structure and narrow pore size distribution. Graphite addition to clay had a positive effect on the support porosity ratio compared with that prepared from pure clay. The present results confirmed the possibility of preparing low-cost ceramic support from raw materials (Tunisian clay) and graphite as the porogenic agent to produce a porous membrane with a porosity of 41% and an acceptable mechanical strength of about 4 MPa using a 15% of graphite addition (G₃) and an 850 °C sintering temperature. The developed tubular support showed high mechanical resistance and presented interesting retention properties with respect to the diesel/water emulsion. The retention rate, evaluated by decreasing turbidity, reached a level of 95%.

ACKNOWLEDGEMENT

The authors wish to express their gratitude to the Ministry of Higher Education and Scientific Research of Tunisia.

REFERENCES

- [1] A. Kayvani Fard, G. McKay, A. Buekenhoudt, H. Al Sulaiti, F. Motmans, M. Khraisheh, M. Atieh, *Materials* **11**, 1 (2018) 74.
- [2] J. Ma, X. Xi, C. He, W. Chen, W. Tian, J. Li, C. Wang, B. Luo, A. Shui, K. Hua, *Ceram. Int.* **45**, 14 (2019) 17946.
- [3] X. Da, X. Chen, B. Sun, J. Wen, M. Qiu, Y. Fan, *J. Membr. Sci.* **504** (2016) 29.
- [4] J. Zhou, Q. Chang, Y. Wang, J. Wang, G. Meng, *Sep. Purif. Technol.* **75** (2010) 243.
- [5] S. Dey, S.N. Roy, S. Majumdar, S. Ghosh, G.C. Sahoo, *Trans. Ind. Ceram. Soc.* **78**, 4 (2019) 187.
- [6] Y.H. Wang, G. Chen, Z.S. Wang, J.W. Liu, P.F. Luo, *Ceram. Int.* **44** (2018) 2077.
- [7] B.K. Nandi, R. Uppaluri, M.K. Purkait, *LWT* **44**, 1 (2011) 214.
- [8] R. Vinoth Kumar, P. Monash, G. Pugazhenth, *Desalin. Water Treat.* **57**, 58 (2016) 28056.
- [9] M. Mohamed, N. Dayirou, H. Mohamed, N. André, L.-N. Gisèle Laure, N. Daniel, *Trans. Ind. Ceram. Soc.* **79**, 1 (2020) 1.
- [10] N. Ahmed, F.Q. Mir, *Trans. Ind. Ceram. Soc.* **80**, 1 (2021) 41.
- [11] C. Wang, T. Kasuga, M. Nogami, *J. Mater. Sci. Mater. Med.* **16** (2005) 739.
- [12] S. Li, C.A. Wang, J. Zhou, *Ceram. Int.* **39** (2013) 8833.
- [13] M.M. Lorente-Ayza, M.J. Orts, V. Pérez-Herranz, S. Mestre, *J. Eur. Ceram. Soc.* **35** (2015) 2333.
- [14] R. Serzane, J. Locs, L. Berzina-Cimdina, R. Sadretdinovs, *Process. Appl. Ceram.* **4** (2010) 231.
- [15] S. Khemakhem, R. Ben Amar, R. Ben Hassen, A. Larbot, A. Ben Salah, L. Cot, *Ind. Ceram.* **24**, 3 (2004) 117.
- [16] H. Baccour, M. Medhioub, F. Jamoussi, T. Mhiri, A. Daoud, *Mater. Charact.* **59** (2008) 1613.
- [17] H. Baccour, M. Medhi, F. Jamoussi, T. Mhiri, *J. Mater. Process. Technol.* **209** (2009) 2812.
- [18] W. Hajjaji, M. Hachani, B. Moussi, K. Jeridi, M. Medhioub, A. López-Galindo, F. Rocha, J.A. Labrincha, F. Jamoussi, *J. Afr. Earth Sci.* **57** (2010) 41.
- [19] B. Moussi, M. Medhioub, N. Hatira, J. Yans, W. Hajjaj, F. Rocha, J.A. Labrincha, F. Jamoussi, *Clay Miner.* **46** (2011) 165.
- [20] N. Kamoun, M.A. Rodriguez, F. Jamoussi, *Bol. Soc. Esp. Ceram. V.* **59** (2020) 25.
- [21] M.M. Frocht, *Strength of materials*, Ronald Press, New York (1951) 175.
- [22] R.I. Yousef, B. El-Eswed, M. Alshaaer, F. Khalili, H. Khoury, *J. Hazard. Mater.* **165** (2008) 379.
- [23] S. Monteiro, C. Vieira, *Appl. Clay Sci.* **27** (2004) 229.
- [24] I. Hedfi, N. Hamdi, M.A. Rodriguez, E. Srasra, *Ceram. Int.* **42**, 4 (2015) 5089.
- [25] M. Arzani, H. Reza, M. Sheikhi, T. Mohammadi, O. Bakhtiari, *Appl. Clay Sci.* **161** (2018) 456.
- [26] S.B. Rekik, J. Bouaziz, A. Deratani, S. Baklouti, *J. Membr. Sci. Technol.* **6** (2016) 1.
- [27] M. Mouiyya, A. Abourriche, A. Bouazizi, A. Benhammou, Y. El Hafiane, Y. Abouliatim, L. Nibou, M. Oumam, M. Ouammou, A. Smith, H. Hannache, *Desalination* **427** (2018) 42.
- [28] N. Kamoun, M.A. Rodriguez, F. Jamoussi, *Desalin. Water Treat.* **57** (2016) 1.
- [29] M.G. Song, S.H. Cho, J.Y. Kim, J.D. Kim, *Korean J. Chem. Eng.* **19**, 3 (2002) 425.

(Rec. 29/09/2021, Rev. 02/03/2022, Ac. 21/03/2022)

